AD-A141 047 EMPIRICAL AND DYNAMIC MODES IN THE CCS (CALIFORNIA CURRENT SYSTEM)(U) NAVAL POSTGRADUATE SCHOOL MONTEREY CA J A SMITH MAR 84 NPS68-84-003 1/1

UNCLASSIFIED F/G 8/3 NL

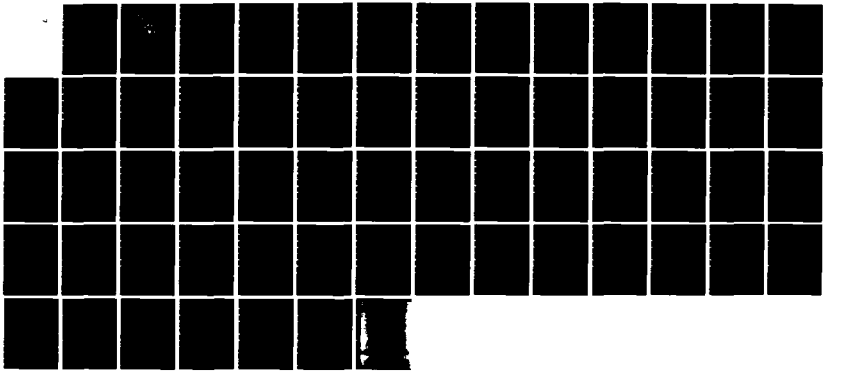

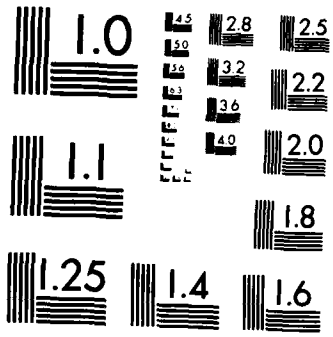

NPS68-84-003

NAVAL POSTGRADUATE SCHOOL

Monterey, California

EMPIRICAL AND DYNAMIC MODES
IN THE CCS

by

JEROME A. SMITH

MARCH 1984

Prepared for:
Office of Naval Research
Environmental Sciences Directorate (Code 420)
Arlington, VA 22217

NAVAL POSTGRADUATE SCHOOL

Monterey, California 93943

Commodore R.H. Shumaker
Superintendent

David A. Schrady
Provost

This report is for the research project "Ocean Prediction Through Observations, Modeling and Analysis" sponsored by the Physical Oceanography Program of the Office of Naval Research under Program Element 61153N.

This report was prepared by:

Jerome A. Smith
Adjunct Prof., Oceanography

Reviewed by:

Christopher N.K. Mooers, Chairman
Department of Oceanography

Released by:

John N. Dyer
Dean of Science and Engineering

SECURITY CLASSIFICATION OF THIS PAGE (When Data Entered)

REPORT DOCUMENTATION PAGE

READ INSTRUCTIONS BEFORE COMPLETING FORM

1. REPORT NUMBER NPS68-84-003	2. GOVT ACCESSION NO. AD-A141047
3. RECIPIENT'S CATALOG NUMBER	
4. TITLE (and Subtitle) EMPIRICAL AND DYNAMIC MODES IN THE CCS	5. TYPE OF REPORT & PERIOD COVERED
	6. PERFORMING ORG. REPORT NUMBER
7. AUTHOR(s) Jerome A. Smith	8. CONTRACT OR GRANT NUMBER(s) 61153N N0001484WR24051
9. PERFORMING ORGANIZATION NAME AND ADDRESS Naval Postgraduate School Monterey, Ca 93943	10. PROGRAM ELEMENT, PROJECT, TASK AREA & WORK UNIT NUMBERS
11. CONTROLLING OFFICE NAME AND ADDRESS Office of Naval Research (Code 420) Arlington, VA 22217	12. REPORT DATE March 1984
	13. NUMBER OF PAGES
14. MONITORING AGENCY NAME & ADDRESS(if different from Controlling Office)	15. SECURITY CLASS. (of this report) UNCLASSIFIED
	15a. DECLASSIFICATION/DOWNGRADING SCHEDULE

16. DISTRIBUTION STATEMENT (of this Report)

Approved for public release;
Distribution unlimited.

17. DISTRIBUTION STATEMENT (of the abstract entered in Block 20, if different from Report)

18. SUPPLEMENTARY NOTES

Portions of this report were presented at the Fall Annual Meeting, AGU, San Francisco, 13 Dec. 1983, and at the Ocean Science Meeting, New Orleans, 27 Jan. 1984

19. KEY WORDS (Continue on reverse side if necessary and identify by block number)

Empirical Orthogonal Functions
Quasi-geostrophic dynamic modes
Modal coupling
XBT data
CTD data
California Current

20. ABSTRACT (Continue on reverse side if necessary and identify by block number)

See reverse side.

DD FORM 1 JAN 73 1473 EDITION OF 1 NOV 65 IS OBSOLETE
S/N 0102-LF-014-6601

UNCLASSIFIED
SECURITY CLASSIFICATION OF THIS PAGE (When Data Entered)

EMPIRICAL AND DYNAMIC MODES IN THE CCS

Jerome A Smith, Department of Oceanography,
Naval Postgraduate School, Monterey, CA 93941

ABSTRACT

CTD data from the California Current System ~~(CCS)~~ are analysed in terms of both empirical orthogonal functions (EOFs) and quasi-geostrophic vertical modes (QGMs). A single EOF accounts for about 97% of the total variance in hydrostatic pressure perturbations to 3000m. The first four pressure EOFs correspond quite well to the first four QGMs. The QGMs are orthogonal with respect to integration over the total water depth, while the EOFs are orthogonal over the depth interval where there are data; thus, as subsets of increasingly deeper cast data are used, the EOFs and QGMs become more alike. The EOF amplitudes must also be uncorrelated over the sample of profiles used, while those of the QGMs need not be; yet, the EOF analysis roughly selects the first four QGMs, even from just eight casts to 3000m. Apparently, the variance contained in each successive QGM decreases precipitously; thus, the variance in QGM 1 overwhelms any correlated part of QGM 2. Likewise, the variance left over in QGM 2 is still sufficient to overwhelm QGM 3 (and so on). (Note also that low-frequency internal waves, e.g. internal tides, have virtually identical modal structure to the QGMs; these may also contribute to the EOFs).

In the upper 100 meters, the EOFs vary markedly from survey to survey. The density analysis can produce an EOF which doesn't fit into the 'normal' QGM sequence, but rather is strongly surface trapped, being confined roughly to the top 100 meters. This mode, which may represent mixed or Ekman layer variability, can account for up to 20% of the total density variance.

Empirical and Dynamic Modes in the CCS

a report prepared in conjunction with

OPTOMA

by

Jerome A. Smith

The **OPTOMA** Program is a joint program of

Department of Oceanography
Naval Postgraduate School
Monterey, CA 93943.

Center for Earth and Planetary Physics
Harvard University
Cambridge, MA 02138.

A1

EMPIRICAL AND DYNAMIC MODES IN THE CCS

Jerome A Smith, Department of Oceanography,
Naval Postgraduate School, Monterey, CA 93941

ABSTRACT

CTD data from the California Current System (CCS) are analysed in terms of both empirical orthogonal functions (EOFs) and quasi-geostrophic vertical modes (QGMs). A single EOF accounts for about 97% of the total variance in hydrostatic pressure perturbations to 3000m. The first four pressure EOFs correspond quite well to the first four QGMs. The QGMs are orthogonal with respect to integration over the total water depth, while the EOFs are orthogonal over the depth interval where there are data; thus, as subsets of increasingly deeper cast data are used, the EOFs and QGMs become more alike. The EOF amplitudes must also be uncorrelated over the sample of profiles used, while those of the QGMs need not be; yet, the EOF analysis roughly selects the first four QGMs, even from just eight casts to 3000m. Apparently, the variance contained in each successive QGM decreases precipitously; thus, the variance in QGM 1 overwhelms any correlated part of QGM 2. Likewise, the variance left over in QGM 2 is still sufficient to overwhelm QGM 3 (and so on). (Note also that low-frequency internal waves, e.g. internal tides, have virtually identical modal structure to the QGMs; these may also contribute to the EOFs).

In the upper 100 meters, the EOFs vary markedly from survey to survey. The density analysis can produce an EOF which doesn't fit into the 'normal' QGM sequence, but rather is strongly surface trapped, being confined roughly to the top 100 meters. This mode, which may represent mixed or Ekman layer variability, can account for up to 20% of the total density variance.

EMPIRICAL AND DYNAMIC MODES IN THE CCS

1. Introduction.

It is useful to examine data in a statistically objective manner, to see what information comes to light without the introduction of prejudice. On the other hand, utilization of dynamic insight should (if correct) improve the accuracy of the analysis and/or prediction of subsequent evolution.

One task in the OPTOMA program (Ocean Prediction Through Observation, Modeling, and Analysis) is to incorporate CTD and XBT survey data (etc.) into a dynamical/statistical analysis and prediction scheme (c.f. Robinson et. *al.* 1984). To this end, it is appropriate to examine both the empirical orthogonal functions (EOFs) and the quasi-geostrophic dynamic modes (QGMs).

The use of EOFs to define vertical structures is particularly attractive in the present case, since a single EOF typically accounts for over 95% of the observed variability in hydrostatic pressure (excluding the unresolved barotropic component). Another advantage of this approach is that it may simplify the estimation of deeper mode structure from shallower density profiles, or even from shallower profiles of T alone (e.g., from XBT data).

The use of QGMs is made necessary by the desire to predict evolution with a quasi-geostrophic numerical model. Thus, the relation between the EOFs derived from CTD data and the corresponding QGMs is explored here. Internal wave activity may also be anticipated, and, in particular, the lower frequency internal waves (e.g. internal tides) have vertical modal structure which is indistinguishable from the QGMs. The problem of separating the quasi-geostrophic and internal wave activity is not pursued here, and, for the purpose of comparison with the EOFs, they will be lumped together in the 'QGMs'.

Each EOF may be projected onto a series of QGMs using (for example) a least-squares fit over the depth range of the EOF (the EOFs only extend as deep as the data, whereas the QGMs extend to the ocean bottom). In addition, the QGMs can be projected onto each other over the same depth range (within which they are not orthogonal). This allows evaluation of how well the EOF analysis separates the QGMs, taking into account the 'crosstalk' between QGMs; i.e., whether the EOFs can be viewed as QGMs 're-orthogonalized' over the depth interval of the data. The QGM amplitudes at any given station can then be estimated in two ways: by direct least-squares fitting of the QGMs over the data depth, or through the EOF amplitudes, using the decomposition of each EOF into QGMs (again via least-squares fitting). In practice, the least-squares method only yields robust results for the deeper data (i.e., 1500 or 3000m casts), and the corresponding deeper EOFs (i.e.,

1500 or 3000m EOFs). Estimation from shallower casts (e.g., 500 or 750m) will require furthur consideration. A method suggested here is to develop empirical correlations between amplitudes of the shallower EOFs and the QGM amplitudes, based on the deeper cast data: e.g., derive shallow EOFs from just the top 500m (say) of all 1500m casts; the amplitudes of these shallow EOFs can then be compared to those of the deeper EOFs, or directly to the amplitudes of the QGMs derived from 1500m fits. The empirical correlations between these different sets of amplitudes can be estimated from all the casts to 1500m, and then used to translate the shallow EOF amplitudes into (deep) QGM amplitudes via traditional objective analysis (along with appropriate error bounds).

To compare the two sets of modes, it is crucial that the constraints applied to both are as similar as possible. The EOFs are defined here to be orthogonal with respect to integration in depth, in a finite-difference approximation; i.e., with respect to summation in depth weighted by layer thicknesses. Unavoidably, the EOFs produced are orthogonal with respect to vertical integration to the depth of the data, whereas the QGMs are orthogonal over the total water depth. Also, the EOFs have uncorrelated amplitudes over the sample of profiles; whereas the QGMs do not necessarily have this property. These differences in the constraints could cause differences between the two sets of modes. The results, however, indicate that this is not the case; i.e., the first four EOFs are remarkably similar to the first four QGMs. The rapid decrease

in observed variance with mode number can help maintain this correspondence: a given EOF may be thought of as a combination of the corresponding QGM and the correlated fraction of higher dynamic modes; the contribution from this latter fraction is then swamped by the much greater variance in the lower mode.

The quasi-geostrophic modes (QGMs) and empirical orthogonal functions (EOFs) are briefly discussed and the constraints governing both are compared. The use of XBT data to estimate dynamic height or to estimate amplitudes of the QGMs is not pursued here (see, e.g., Stommel 1947, Emery 1975, Emery and Wert 1976, or Flierl 1978a for some discussion of the use of XBT data to estimate dynamic height). Also, the questions of how to extrapolate/interpolate in time and space, how to separate internal wave and quasi-geostrophic activity, or how to implement the results in a numerical model, are left open (see, e.g., McWilliams 1976, McWilliams and Flierl 1976, Flierl 1978b, McWilliams and Shen 1980). The EOF/QGM analysis is applied to recent survey data.

II. The Data.

The data were acquired in surveys conducted in connection with the OPTOMA program. The region in which these surveys have been conducted extends roughly from 100 to 300 kilometers offshore from California, and between 35 and 40 N (see Figure 1). These surveys consist of mixed CTD and XBT casts; only the CTD data are considered

CTD STATIONS

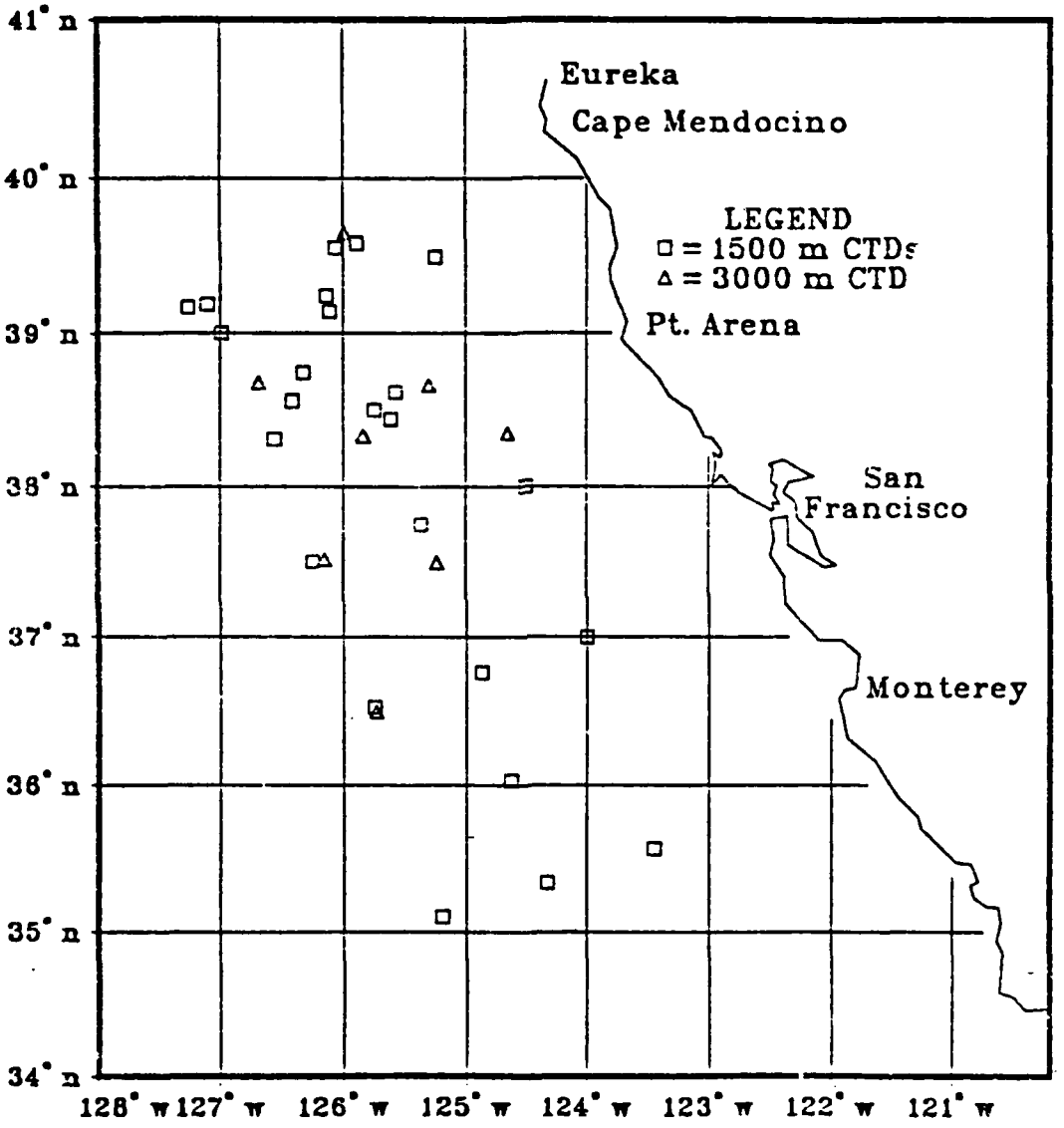

1 Locations of the 1500m and 3000m CTD casts.

here. Surveys including CTD data were conducted in August 1982 (designated OPTOMA2), March 1983 (OPTOMA4-1 and -2), and in June-July 1983 (OPTOMA5-D, OPTOMA5-A1, and OPTOMA5-A3). Of the total of 169 CTD casts extending to at least 500 meters, 33 reach to 1500m, and 8 casts reach to 3000m (see Table 1). For comparison, the N^2

Table 1.

(breakdown of CTD stations by survey)

survey:	opt2	opt4-1	opt4-2	opt5-a1	opt5-a3	opt5-d
>500m CTDs	66	25	26	6	18	28
>1500m CTDs	9	8	8	-	-	8
>3000m CTDs	-	-	-	-	-	8

profiles for each survey are shown in Figure 2.

OPTOMA2 consists of two mappings of roughly the same area (between 37.5 and 40 N, henceforth denoted NOCAL) conducted within a total span of about six days; weather conditions were fairly typical for the region, with only moderate weather systems before and during the survey. This data set is also described elsewhere (Mooers and Robinson 1984, Rienecker *et al.*, 1984).

OPTOMA4-1 was conducted following a storm (in NOCAL), as is apparent from the appearance of a deep, well formed mixed layer. OPTOMA4-2 was conducted the following week, during mild, sunny

$N^2(z)$ from each survey

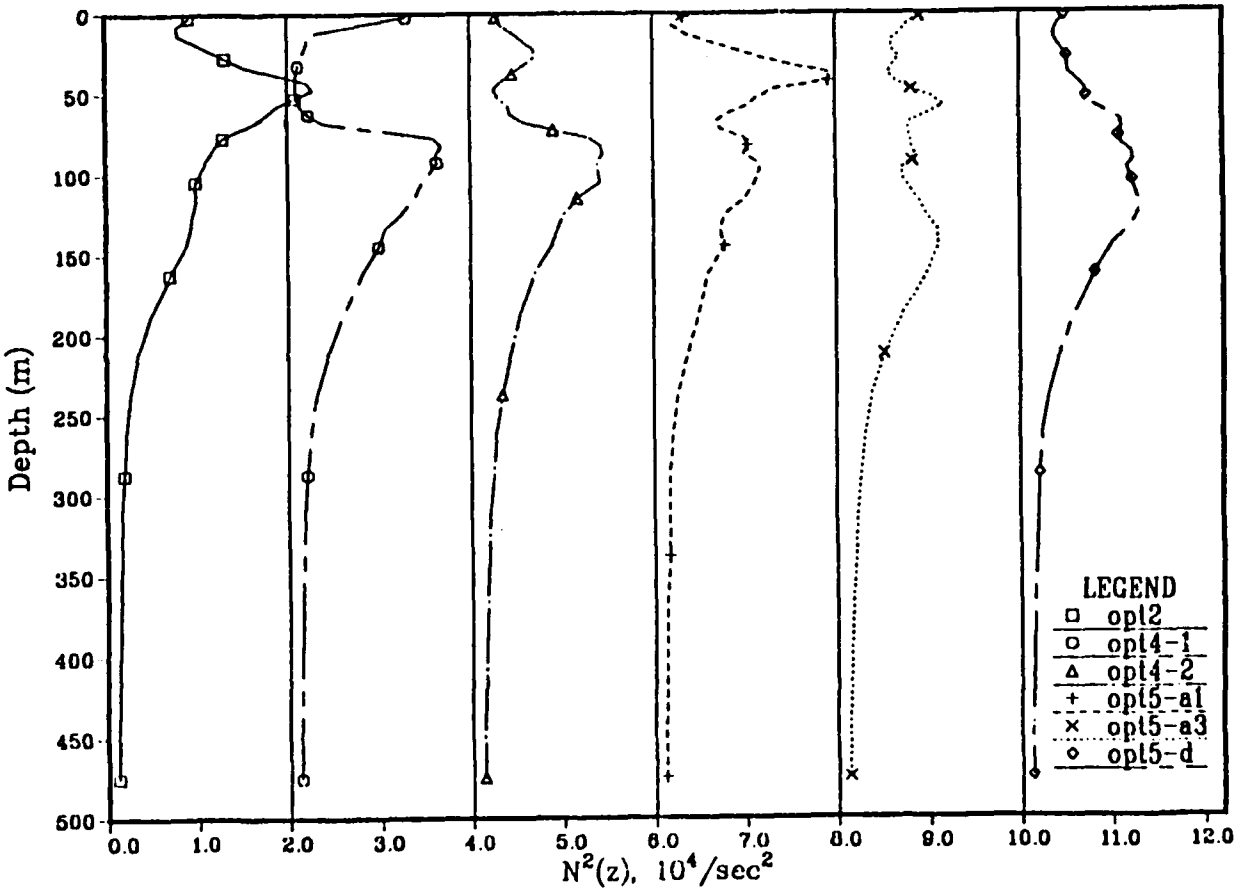

2 Buoyancy frequency profiles from each survey, using all CTD data to 500m or greater. Note the well-mixed layer in the top 100m of OPTOMA4-1.

conditions. Although the domain is different from OPTOMA4-1 (between 35 and 37 N, denoted 'CENCAL'), the results are consistent with re-stratification of the surface layer.

OPTOMA5 represents the most ambitious experiment to date in the OPTOMA Program. OPTOMA5-D is a large scale survey conducted with the R/V De Steiguer, extending across both NOCAL and CENCAL. In OPTOMA5-A1, A2, and A3, the R/V Acania re-surveyed a domain about 120 kilometers square (in NOCAL), starting 14 days apart. Each survey took about 5 days, and the first (A1) overlapped the De Steiguer survey in both time and location. OPTOMA5-D and OPTOMA5-A1 took place after and during a period of typical conditions. The eight casts to 3000 meters were taken aboard the De Steiguer; the R/V Acania is at present configured for a maximum depth of 1500 meters. After the sixth CTD cast in OPTOMA5-A1, a storm moved in, preventing any further CTD stations from being taken, and creating a moderately deep mixed layer. No CTD casts were made during OPTOMA5-A2 (due to a winch failure); however, the XBT data indicate that the near-surface layer became re-stratified, due to the mild weather encountered. OPTOMA5-A3 was conducted during continued mild conditions, and the data indicate little or no surface mixed layer.

The data were processed as follows: salinity (S) was calculated from temperature (T) and conductivity (c.f. Lewis and Perkin 1978), the T and S profiles were reduced to 5 meter vertical resolution, and then the

down and up casts were averaged, when both were available (the processing to this point, including position checking, etc., was performed by Dr. M. M. Rienecker and Ms. M. C. Colton at NPS). Sigma-T profiles were calculated using the UNESCO 1980 equations of state (Millero et al., 1980) and the temperature and sigma-T profiles were de-spiked with a 3-point median (Tukey) filter, and smoothed with a 1/4-1/2-1/4 filter. The sigma-T profiles were then modified to eliminate static instabilities, by imposing the condition that successively shallower samples are not denser than the previous ones, working up from the bottom (salinity is not considered further here). The total number of allowed sampling depths was then reduced to 64, spanning 0 to 4500 meters depth, by increasing the sampling interval with depth (in deference to the decrease with depth of the variances of density and temperature). The sample intervals used, starting at the surface, are: 5m (to 100m), 10m (to 150m), 25m (to 350m), 50m (to 800m), 100m (to 2000m), 250m (to 3500m), and 500m (to the bottom). The value at each resulting 'target depth' was chosen by (a) defining new intervals surrounding each target depth, using the midpoints between target depths, (b) fitting a straight line to all available data in the interval surrounding the target depth, and (c) taking the value given by the line at the target depth. This decimation of the data enabled the analysis programs to run on NPS's IBM 3033 with little difficulty.

To keep the discussion simple, no distinction will be made between true density profiles (including adiabatic and isothermal compression effects) and sigma-T profiles. The distinction is, in any case, negligible in all but the deepest (3000m) data.

III. The Dynamic modes.

To facilitate computation, and to speed the production of analysis/forecast maps, the dynamic model employed in the OPTOMA project makes use of the quasi-geostrophic (QG) approximation (see Miller, Robinson, and Haidvogel 1983 for a description of the numerical model). In this approximation, potential vorticity is conserved along streaklines; the QG potential vorticity 'ζ' is given by

$$\zeta = \nabla_H^2 \psi + \beta y + \frac{\partial}{\partial z}\left(\frac{f^2}{N^2}\frac{\partial}{\partial z}\psi\right),$$

where ∇_H^2 is the horizontal Laplacian operator, $\psi(x,y,z,t)$ is the streamfunction for horizontal velocity, β is the north-south derivative of the coriolis parameter, f, and N(z) is the mean buoyancy frequency profile. In this equation, the first term on the right is the relative vorticity; the second represents the variation of planetary vorticity with latitude (or "y"); and the last term gives the contribution due to vortex stretching acting on the planetary vorticity.

The last term, the "stretchiness", is the only term which explicitly involves vertical variations. It is conventional to separate the vertical from the horizontal and time dimensions by describing the streamfunction

ψ as a sum of quasi-geostrophic modes or "QGMs", $\varphi_m(z)$. The modes φ_m are eigenvectors of this "stretchiness" term:

$$\frac{\partial}{\partial z}\left(\frac{f^2}{N^2}\frac{\partial}{\partial z}\varphi_m(z)\right) = -\lambda_m^2 \varphi_m(z), \quad 0 < z < H^T,$$

subject to the boundary conditions (for flat top and bottom),

$$\frac{\partial}{\partial z}\varphi_m(0) = \frac{\partial}{\partial z}\varphi(H^T) = 0.$$

The eigenvalue λ_m^2 corresponds to the squared inverse of the n-th internal Rossby radius of deformation (the barotropic mode is here denoted as the 0-th mode, φ_0, so that the first baroclinic mode is φ_1). The streamfunction $\psi(x,y,z,t)$ is hence described by the infinite sum

$$\psi(x,y,z,t) = \sum_{m=0}^{\infty} A_m(x,y,t)\,\varphi_m(z),$$

which is truncated at a finite value m=M, governed by a balance between desired vertical resolution, anticipated decrease in A_m with mode, and computational burden. As time evolves, the QGMs φ_m can interact via the non-linear horizontal advection terms in the QG vorticity equation.

To calculate the QGMs from the data, the buoyancy frequency N(z) is derived from the mean density profile, and then extrapolated to the ocean bottom (at 4000m depth) by fitting an exponential tail to the deepest 5 values obtained from the data (roughly, from 800 to 1500m for the 1500m data, or 1800 to 3000 meters for the 3000m case). A finite difference approximation to the above is then solved via a standard eigensystem algorithm (Smith et al., 1976). The density QGMs are obtained by differentiating the pressure QGMs.

The first four baroclinic QGMs are shown in Figures 3 (pressure) and 4 (density). Note the relatively shallow zero crossings of the second and higher modes. The first mode crosses zero at about 1200m depth, the second at only 225m, the third around 130m, and the fourth mode crosses zero as shallow as 100 m depth. Such shallow zero-crossings point to the possible importance of near-surface mixing effects to the overall energetics of the QG motion.

To give an idea of the variability and associated uncertainty, the top 500m of the first density QGM is shown from each survey (Figure 5). The density QGMs vary significantly between surveys within the top 100m or so; this is clearly related to the varying 'mixed layer' conditions, combined with the relatively strong surface-trapping of the modes.

To anticipate the difficulties to be encountered in fitting EOFs of various depths by the QGMs, it is worthwhile to examine the "crosstalk" between the QGMs over the desired depth intervals. The pressure QGMs are orthonormal over the total water depth,

$$\int_0^{H^T} \varphi_m(z)\,\varphi_n(z)\,dz = H^T \delta_{mn} ,$$

where H^T is the total water depth (normalizing to the depth H^T will facilitate comparison with EOFs formed to the different depths H^P). The density QGMs, $\varphi'_m(z)$, are orthonormal with respect to a weighted integration, where the weighting is by N(z); i.e., replace $\varphi_m(z)$ in the above by $N(z)\varphi'_m(z)$. The EOFs are orthonormal only over the depth

Q–G Pressure modes

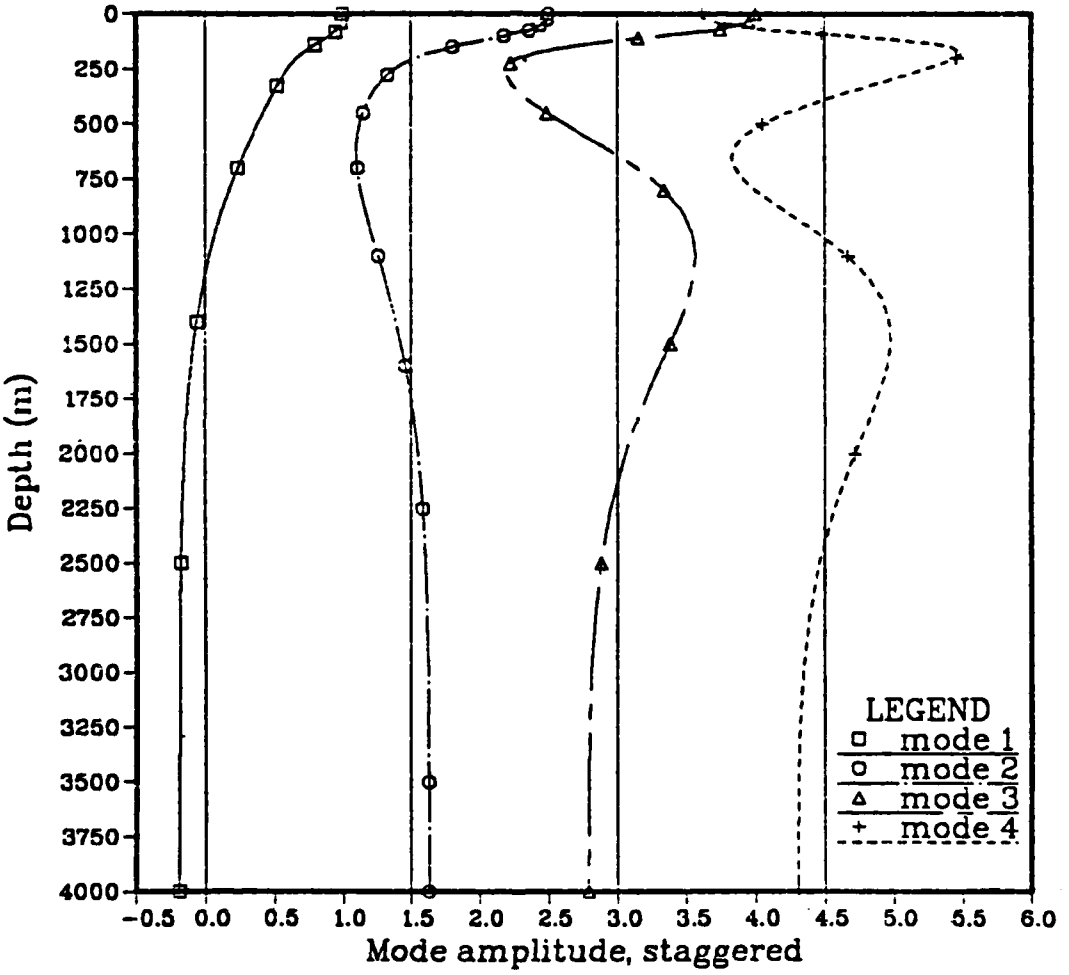

3

The first four quasi-geostrophic modes (QGMs) for hydrostatic pressure, calculated from the overall mean buoyancy profile.

Q–G Density modes

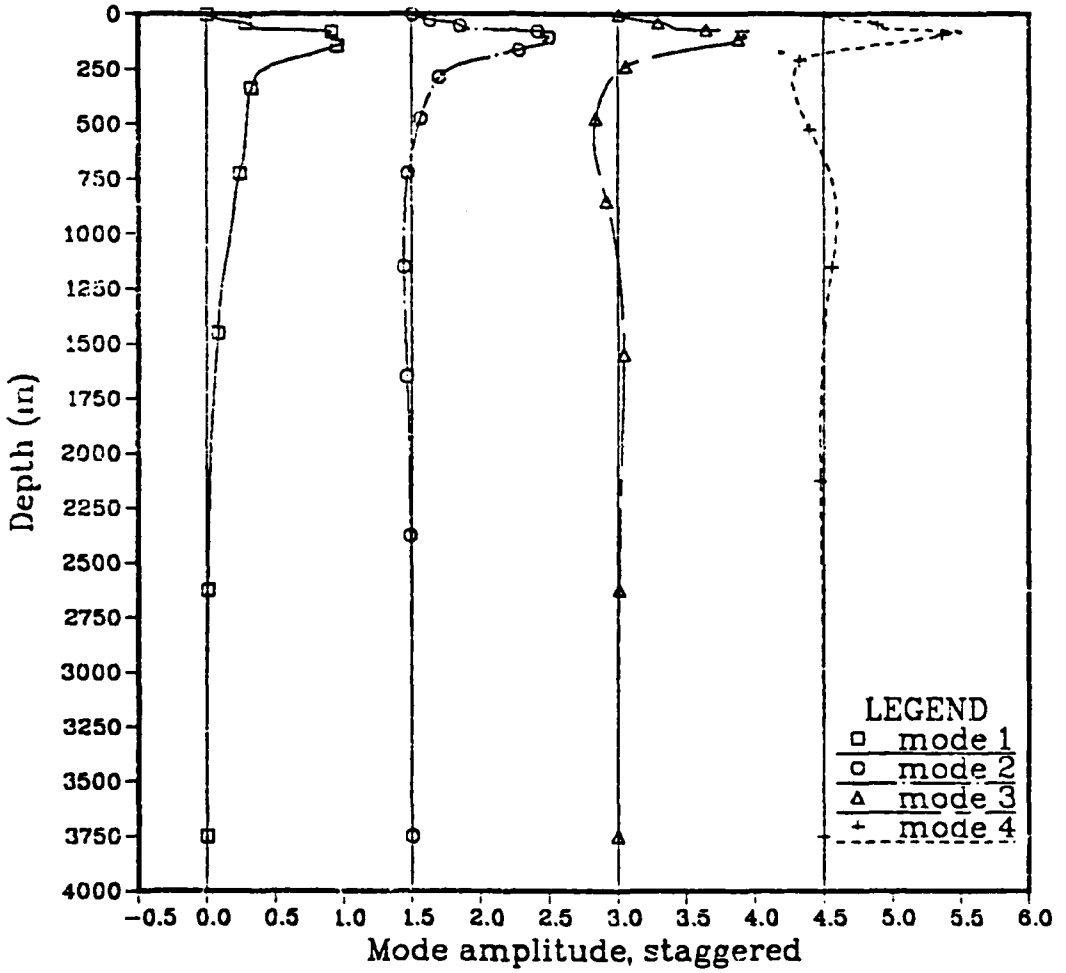

4 The first four quasi-gestrophic modes for density.

Q-G Density Modes from each survey

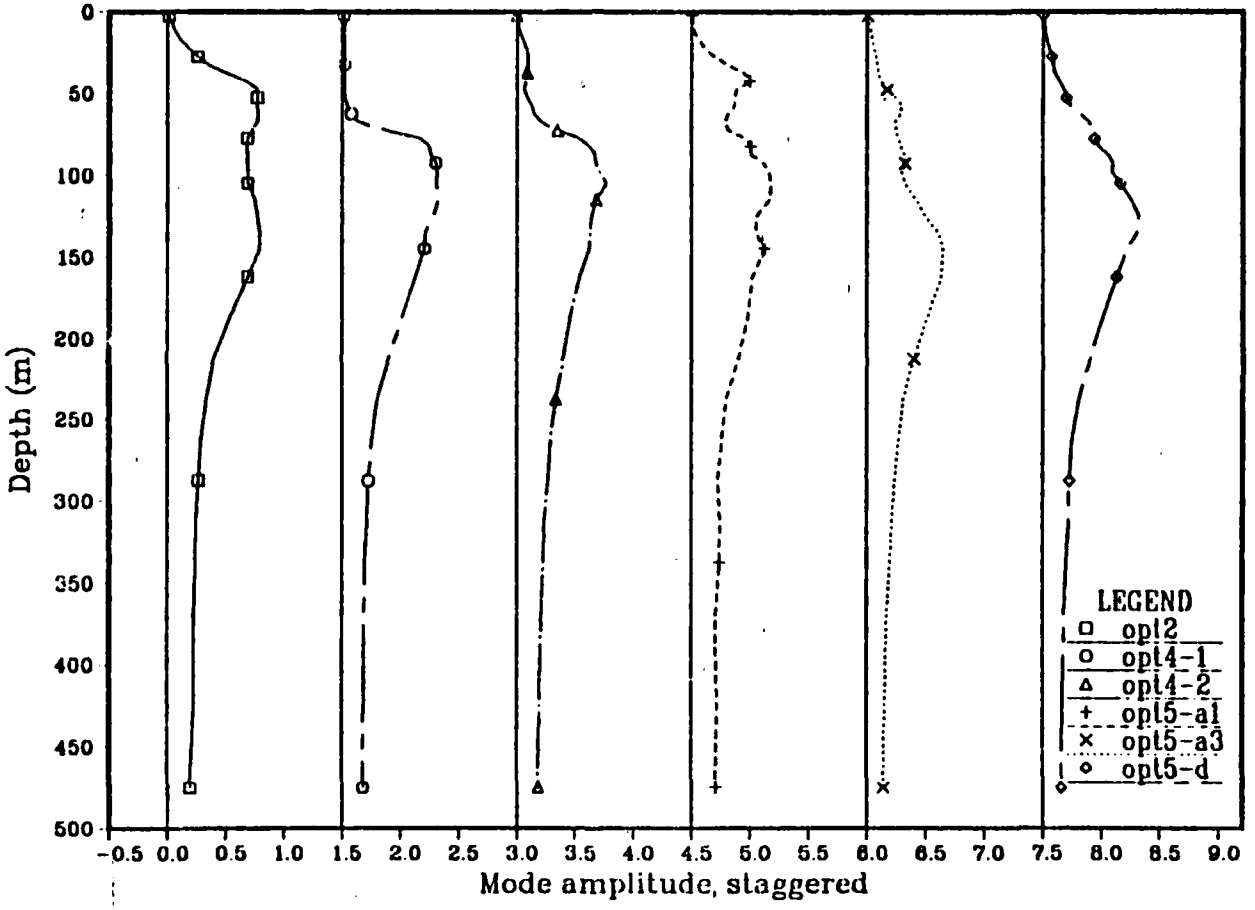

5 The first density QGM from each survey, using all casts to 500m or greater. Note the variations in the top 150m or so.

range H^2 where there is data. Also, the effects of near-surface mixing may "contaminate" both the EOFs and QGMs in the top few tens of meters (from Figure 5, for example, the top 100m or so are suspect). The desired depth intervals therefore extend from some mixed layer depth to the depth of data being considered (e.g., 100 to 500m; 0 to 3000m; etc.). Over these intervals, the QGMs are not orthogonal; therefore, the EOFs are projected onto the QGMs via least-squares. A finite-difference approximation to a continuous least-squares fit is employed, using layer thicknesses defined by taking the midpoints between sample depths as the layer boundaries. First, this procedure is applied to the QGMs to determine 'crosstalk'. Table 2 shows the 'goodness of fit' of mode 2 by modes 0 and 1, mode 3 by 0 through 2, and of mode 4 by modes 0 through 3. The 'goodness of fit' is defined here as the percentage of variance of a mode within the specified depth range (i.e., of it's squared integral over that range) which is accounted for by a combination of other modes. From these values, it is plausible that the 1500m and 3000m data can be used to resolve the first few modes; however, it is doubtful that QGM 2 or higher will be distinguishable from just the top 500m of data.

Table 2.

QGM crosstalk over various depth intervals

(fit of pressure mode N by modes 0 through N-1)

mode:	2	3	4	5
depth interval:				
100 to 500m	94.8%	99.2%	99.7%	99.95%
100 to 1500m	64.9%	81.2%	85.5%	89.0%
100 to 3000m	21.7%	29.1%	32.1%	41.8%

IV. EOF Analysis.

(A) Description.

Empirical Orthogonal Functions (EOFs) may be defined as the set of orthonormal functions which, for any ordered subset "N", describe the maximum possible portion of observed variance (Lorenz 1956). For example, in describing the deviations from a mean profile of density, the first EOF is a profile of density variations which, by simply being multiplied by a different coefficient for each sample profile, describes the greatest possible fraction of the total density variance. The second EOF then accounts for a maximal fraction of the remaining variance, subject to orthogonality to the first EOF. It also follows that the amplitudes of the EOFs are uncorrelated over the sample population of profiles from which the EOFs were derived (Lorenz 1956; see also Mardia, Kent, and Bibby 1979).

It is tempting to attach dynamical significance to the patterns revealed by the EOFs. This can be misleading, however, since several distinct physical processes could be present which, over the particular stations and depths considered, may not satisfy all the above (rather strong) constraints of orthogonality and statistical independence. It is precisely this question which is addressed in the present comparison between the EOFs and QGMs. In addition, for this comparison to be sensible, the data must be representative of the area in general; i.e., they are tacitly assumed to be statistically homogeneous and stationary.

Mathematically, the EOFs are the eigenvectors of the covariance matrix formed between the various sampling locations. In the present analysis, we wish to approximate the results which would be obtained using continuous profiles; hence, instead of a covariance matrix C_{ij}, we envision a "covariance surface", $C(z,z')$, describing continuously the covariances of density variations at depth z with those at depth z'. Thus we seek EOFs $e_k(z)$ which satisfy:

$$\int_0^{H^P} e_k(z')\, C(z,z')\, dz' = v_k^2\, e_k(z)$$

(where H^P is the depth to which the data extends). In a finite difference approximation, this becomes

$$\sum_{i=1}^{P} e_k(z_i)\, C_{ij}\, h_i = v_k^2\, e_k(z_j)\,,$$

where h_i is the thickness of the layer surrounding z_i (defined here by placing the boundaries midway between the z_i's). The eigenvalue v_k^2 is the "captured variance" corresponding to the k-th EOF e_k. Thus the

EOFs we seek are approximately the eigenvectors associated with a weighted covariance matrix, $h_i C_{ij}$. Since the layer thicknesses are not, in general, equal, this can produce an asymmetric matrix. (However, the same results, within roundoff, are obtained by (1) multiplying each datum by the appropriate root layer thickness, (2) forming the symmetric covariance matrix, (3) solving this eigensystem, and (4) dividing each component of the resulting eigenvectors by the root layer thickness.)

The EOFs satisfy the constraint of orthonormality over the depth range of the data, in the finite difference approximation:

$$\sum_{i=1}^{p} h_i e_k(z_i) e_j(z_i) = H^p \delta_{jk}$$

(normalizing to the data depth 'H^p' facilitates comparison of EOFs formed to different depths). Now consider the actual density perturbation data (i.e. with the mean removed) for the n-th profile:

$$\sigma_n'(z_i) = \sigma_n(z_i) - \bar{\sigma}(z_i)$$

where

$$\bar{\sigma}(z_i) \equiv \frac{1}{N} \sum_{n=1}^{N} \sigma_n(z_i)$$

is the mean profile over the N profiles used. The EOF amplitudes (or 'principal components') a_{nk} may be found using the orthonormality of the e_k's:

$$a_{nk} = \frac{1}{H^p} \sum_{i=1}^{p} e_k(z_i)\, \sigma_n'(z_i)\, h_i \quad ,$$

and these satisfy:

$$\sigma_n'(z_i) = \sum_{k=1}^{p} a_{nk} e_k(z_i)$$

and

$$\sum_{n=1}^{N} a_{nk} a_{nj} = v_k^2 \delta_{kj} \, .$$

The covariance matrix C_{ij} is then given by

$$C_{ij} = \frac{1}{N} \sum^{N} \sigma_n'(z_i)\, \sigma_n'(z_j) \, ,$$

where N is the number of profiles from which the EOFs are to be derived (the alternative symmetric covariance matrix is similar to the above, but with $\sigma_n'(z_i)$ and $\sigma_n'(z_j)$ pre-weighted by $h_i^{1/2}$ and $h_j^{1/2}$, respectively).

In general, to obtain P distinct eigenvalues (and EOFs) requires $N > P+1$. For smaller numbers of profiles, the covariance matrix C_{ij} will have (P+1-N) degenerate eigenvalues. For example, as in the case at hand, there are 50 sample depths from 0 to 1500 meters, but only 33 casts (P=50, N=33); worse yet, there are only 8 casts to 3000m (P=59, N=8). Fortunately, only the few largest eigenvalues are of interest here, and packaged routines exist which seek only the 'M' largest eigenvalues and the associated vectors (see B.T. Smith et. al., 1976). Alternatively, the covariance matrix can be preconditioned by increasing the diagonal elements by some small amount (equivalent, conceptually, to adding some white noise to the data). This second alternative was applied to some of the cases shown (each diagonal element multiplied by 1.000001), and (as expected) yields values and vectors identical to those obtained by the other method (within roundoff error).

(B) Error Bounds.

Setting error bounds on the shapes and eigenvalues of EOFs is not straightforward; indeed, it is an ongoing research topic in modern statistics. The method settled upon here is known as 'the bootstrap' (c.f. Diaconis and Efron 1983, Efron 1979). This method consists of (1)

using a random number generator to draw a resample of N new profiles, with replacement, from the original N profiles (so that, for example, the resample may have more than one copy of some profiles, and none of others); (2) performing the analysis on this resample as was done for the original sample; (3) repeating steps 1 and 2 many times (e.g., 300 times); and (4) using the resulting distribution of results to define confidence limits. The primary advantage of this technique is that it requires no *a priori* assumption about the forms of the distributions of the various quantities of interest (the only assumption is that the original sample is representative of the actual data distribution). The primary disadvantage is computational burden (a typical bootstrapped EOF analysis, resampling 300 times, took about 200 cpu seconds on the IBM 3033).

In applying this method to the present EOF analysis, several concerns arose:

(1) Should a mean profile be recalculated for each resample?

Since the purpose of the bootstrap is to define the variations about the original values, it is desirable that the mean values from the bootstraps be close to the originals (e.g., that the mean shape of EOF 1 from the bootstraps resemble EOF 1 from the original). This correspondance is only maintained if the original perturbations are used throughout (i.e., the answer is 'no').

(2) Does each resample have enough *different* casts to define the fourth EOF? (especially for the 8 deepest casts).

This may be a serious theoretical problem. Since the original mean is used, only four independent casts are required to define a fourth EOF. Resampling eight times from eight casts, the odds are only about 2 in 100 that fewer than 4 casts are chosen. For the present purposes, these 2% or so of the possible 'distributions' were simply rejected.

(3) The bootstrapped eigenvalues associated with a given shape may vary sufficiently from resample to resample that the order in which the shapes are presented may change. In addition, the shapes can vary enough so that the value at any particular depth may cross zero and hence change sign. Hence, which resample EOF goes with which original EOF, and with what sign?

This was most noticeable among the 3000m bootstraps, which were chosen from only 8 original samples. Presumably, such swapping and variability occur further out on the statistical 'tails' for the shallower analyses, due to the increased sample size. To solve this puzzle, the (properly weighted) dot products between each pair of prospective matches were formed. Starting with the original EOF 1, the dot product was formed with each of the resample EOFs. The dot product with greatest magnitude indicates the best resample EOF 1, and the sign of the dot product determines the best sign to apply to it in the comparison. The selected EOF was removed from the pool, and EOF 2 was then selected; etc. (The computational time required for this 'mix and match' is negligible compared to the eigenanalysis.)

(4) The variance near the surface is erratic from resample to resample, so the normalization of the EOFs over total depth will cause variations at depth which may be due entirely to the variations near the surface.

To eliminate this problem, after selection (as in 3), the EOFs were weighted by the root of the associated dimensional eigenvalue, corresponding to the integrated dimensional variance (e.g., of density) explained by the mode over the depth of the data. (The eigenvalues as presented here are normalized by the total variance, equal to the sum of all the eigenvalues; i.e., they are given in terms of percent of the total.)

(C) Application.

The above procedure was applied to the data $\sigma_n(z_i)$ in two ways: (1) to the (demeaned) profiles $\sigma_n'(z_i)$, and (2) to profiles of baroclinic hydrostatic pressure variations,

$$p_n(z_i) = g \sum_{j=i}^{P} h_j \sigma_n'(z_j),$$

where g is gravity and h_j is the thickness of the layer surrounding z_j. This second option (pressure EOFs) should correspond directly to the quasi-geostrophic streamfunction $\psi(z)$ (through a factor $1/\rho_o f$). The first option (density EOFs) should correspond to the vertical derivative of $\psi(z)$. To preserve the similarity between the EOFs and the QGMs, the density EOFs (option 1) were formed by first weighting the density data at each level by N(z), performing the eigenanalysis, and then unweighting the resultant EOFs.

In each case, only profiles reaching at least to the desired depth $z_2 = H^2$ were used. Although a mean profile and a correlation matrix can be formed from casts to varying depths, by using however many products exist between each pair of depths, this may be unwise. For example, if the casts to 1500m happen to occur more frequently within "warm features" than the shallower casts, this causes a shift in the mean profile at that depth; this, in turn, introduces artificial discontinuities in the demeaned data from the deeper casts, as used to derive the EOFs.

The first four modes for pressure are shown in Figures 6 (to 3000m, based on 8 casts) and 7 (to 1500m, based on 34 casts). In both cases, the depth-mean pressure was removed from each station profile before forming the correlations; this ensures orthogonality with respect to the unresolved barotropic mode, and hence helps to maintain the similarity of the constraints applied to the EOFs and QGMs. The traditional level of reference approach may also be used (note that QGM 1 has a zero crossing near 1500m; also note that the first four 3000m EOFs all have zero crossings near 1500m).

The most striking feature of these results is the similarity of the pressure EOFs to the QGMs (Figures 3 and especially 6). It is surprising that eight profiles to 3000m can produce four reasonable looking EOFs, which (furthermore) roughly agree in shape with the QGMs. Presumably this is possible because of the overwhelming proportion of variance in each successive mode (see discussion): in

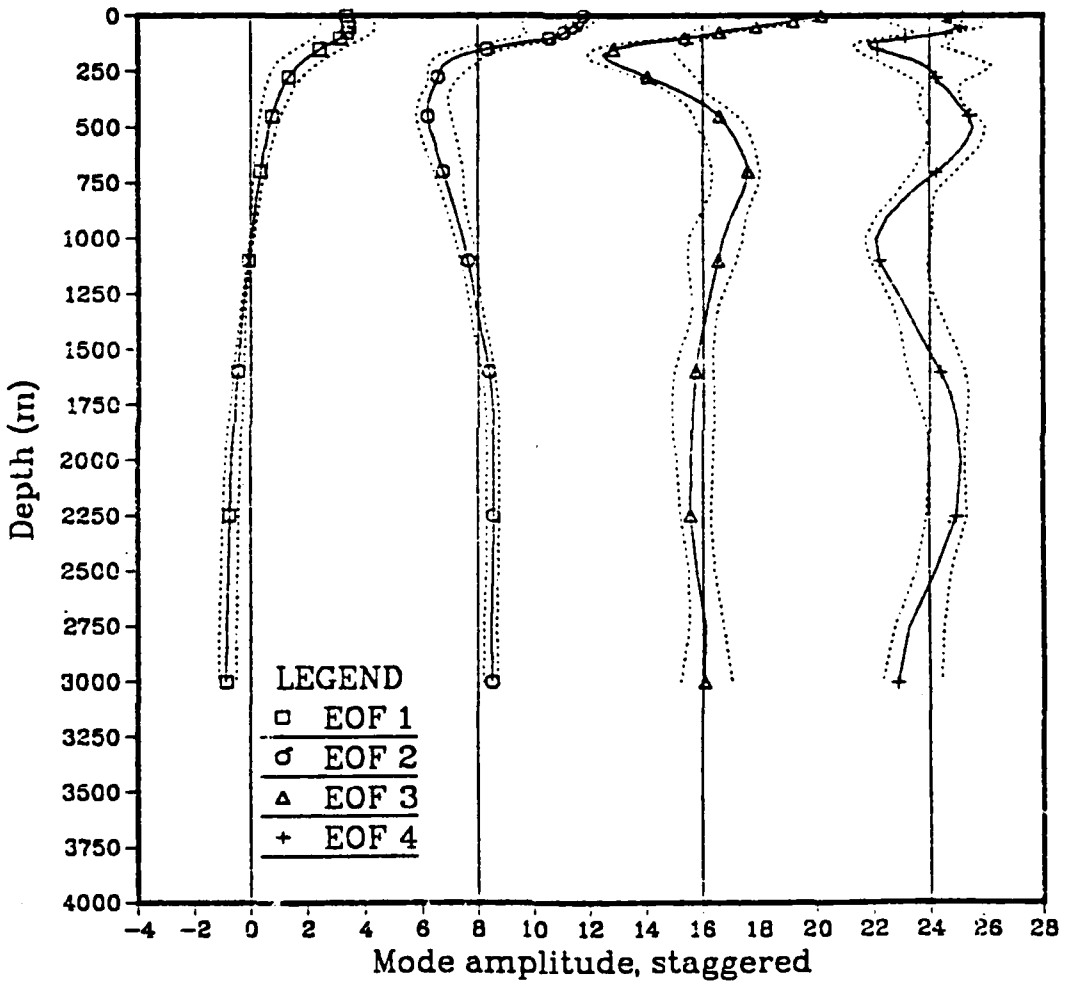

6 The first four empirical orthogonal functions (EOFs), from just the eight casts to 3000m. The confidence limits are estimated by 'bootstrap'. Note the similarity to the QGMs (Figure 3).

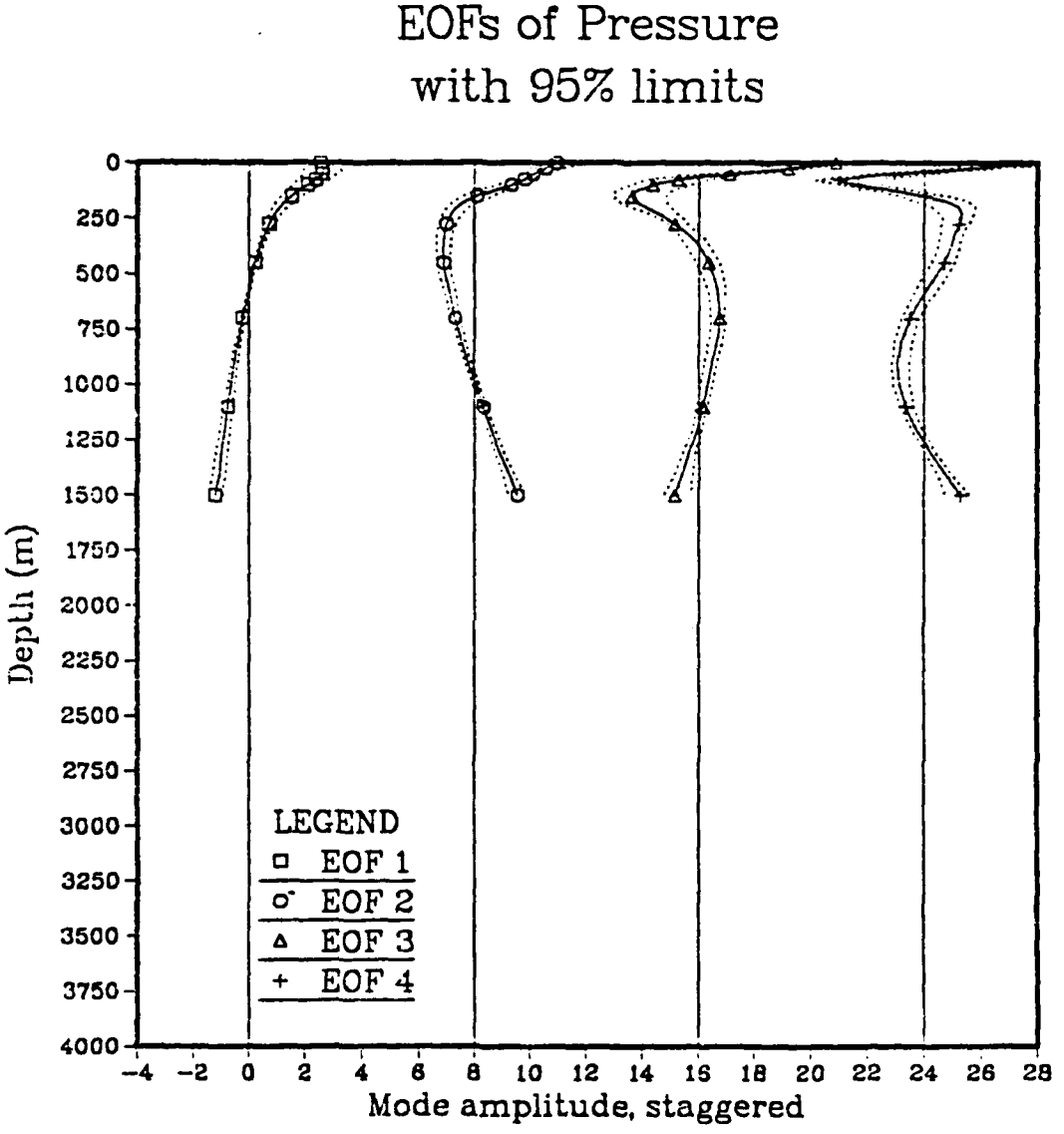

7 The first four EOFs of hydrostatic pressure variations, from all 33 casts to 1500m or greater.

terms of hydrostatic pressure, EOF 1 accounts for 96.7% of the total variance to 3000m; of the remaining 3.3%, EOF 2 accounts for 77%; of the remaining 0.74%, EOF 3 accounts for 59%; of the last .30%, EOF 4 accounts for 61%. If the definition of structure to greater depth is taken to be more important than the sampling error introduced by using only eight casts, or likewise if the enforcement of the orthogonality condition to a depth nearer the total depth is important, interest will naturally fall mostly upon these 3000 meter results. Luckily, as mentioned above, these eight casts were taken during 'quite typical conditions', and so probably do represent a fairly typical distribution of data.

The density modes are shown to 1500m in Figure 8. The percentages of total variance captured by each are, in descending order, 66.4%, 17.5%, 8.4%, and 3.7% (i.e., each mode captures about half of the remaining variance). A feature of note here is the second density EOF. Unlike in the pressure case, QGM 2 for density is similar to EOF 3 (compare Figures 4 and 8). The extra mode (EOF 2) is quite strongly surface trapped, which is suggestive of some kind of "mixed layer mode". This strong surface trapping also helps account for the fact that the analogous mode does not appear among the first 4 pressure EOFs: the operation of integration tends to de-emphasize spiky features.

To help decide which of the EOFs are 'significant' (in the sense of being unlikely to arise from noise), it is useful to examine the sequence

EOFs of Density with 95% limits

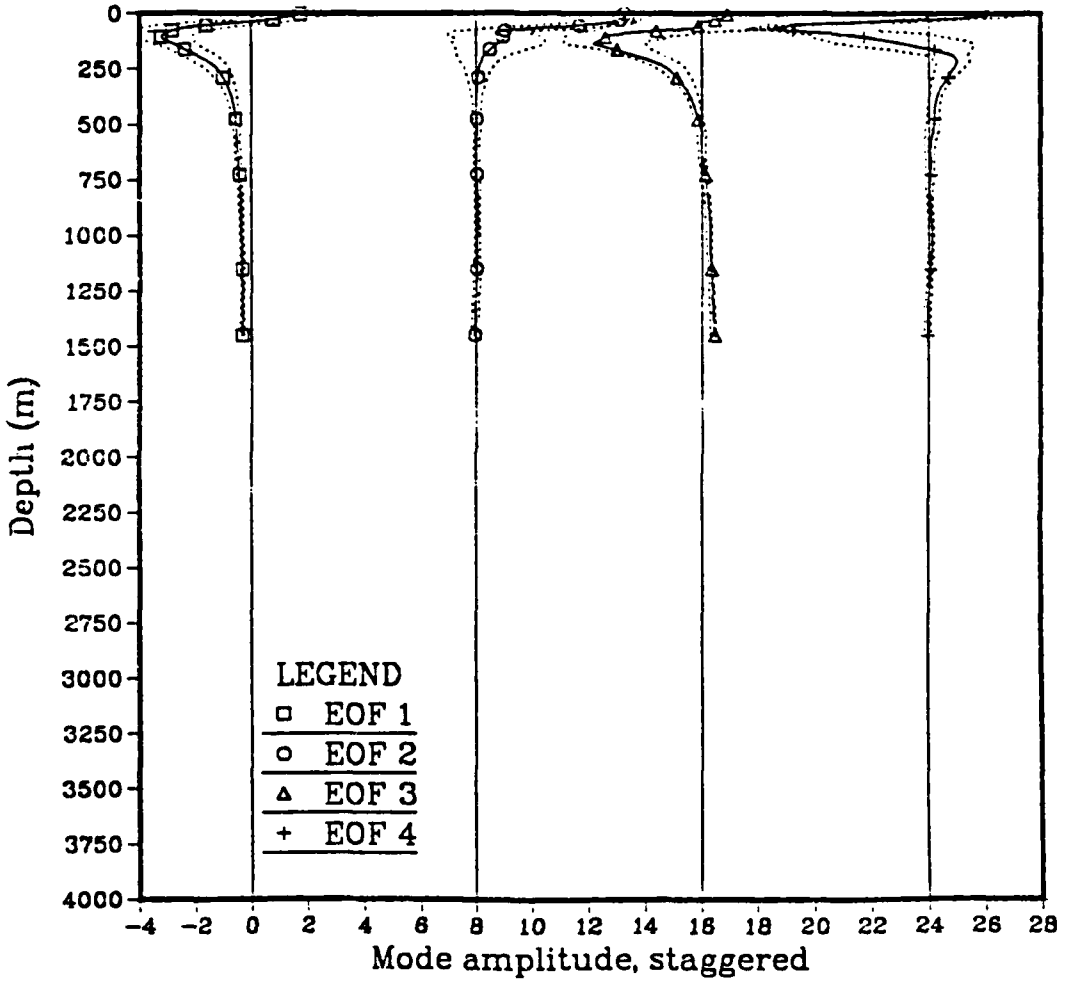

8 The first four EOFs of density variations, from all 33 casts to 1500m. Note the surface-trapped second mode. This mode alone has no QGM analogue; however, it can account for up to 20% of the total density variance.

of eigenvalues ('captured variances'). To put each successive eigenvalue on a more equal footing, each is here compared to the 'residual variance'; i.e., with the variance accounted for by lower modes subtracted out. Thus, the first eigenvalue was divided by the total variance, the second by the total *minus* the first eigenvalue, *et cetera*. To provide confidence limits on these curves, the 'bootstrap' was applied (see last section). For comparison, sets of N 'profiles' of random numbers were generated, having the same variance at each depth as the data, but with no true correlation between depths. The analysis (including, if appropriate, integration in depth) was then repeated on 300 such sets of profiles, to form a Monte Carlo estimate of the confidence limits on the equivalent eigenvalues generated by noise. The resulting curves of the fraction of residual variance accounted for by each mode, for both the real data and the Monte Carlo data, are shown in Figures 9 and 10 (for the 1500m EOFs of pressure and density, respectively). The curve for the 3000m pressure EOF (not shown) indicates that the third and fourth eigenvalues are near the 95% limit for noise, and so should be considered with some reserve. It should be re-iterated that a principle source of noise, internal waves, has virtually the same vertical modal structure as the QGMs, and it does not appear as noise in this comparison. However, these figures indicate that the data is otherwise remarkably noise-free: note that the 95% limits do not even overlap.

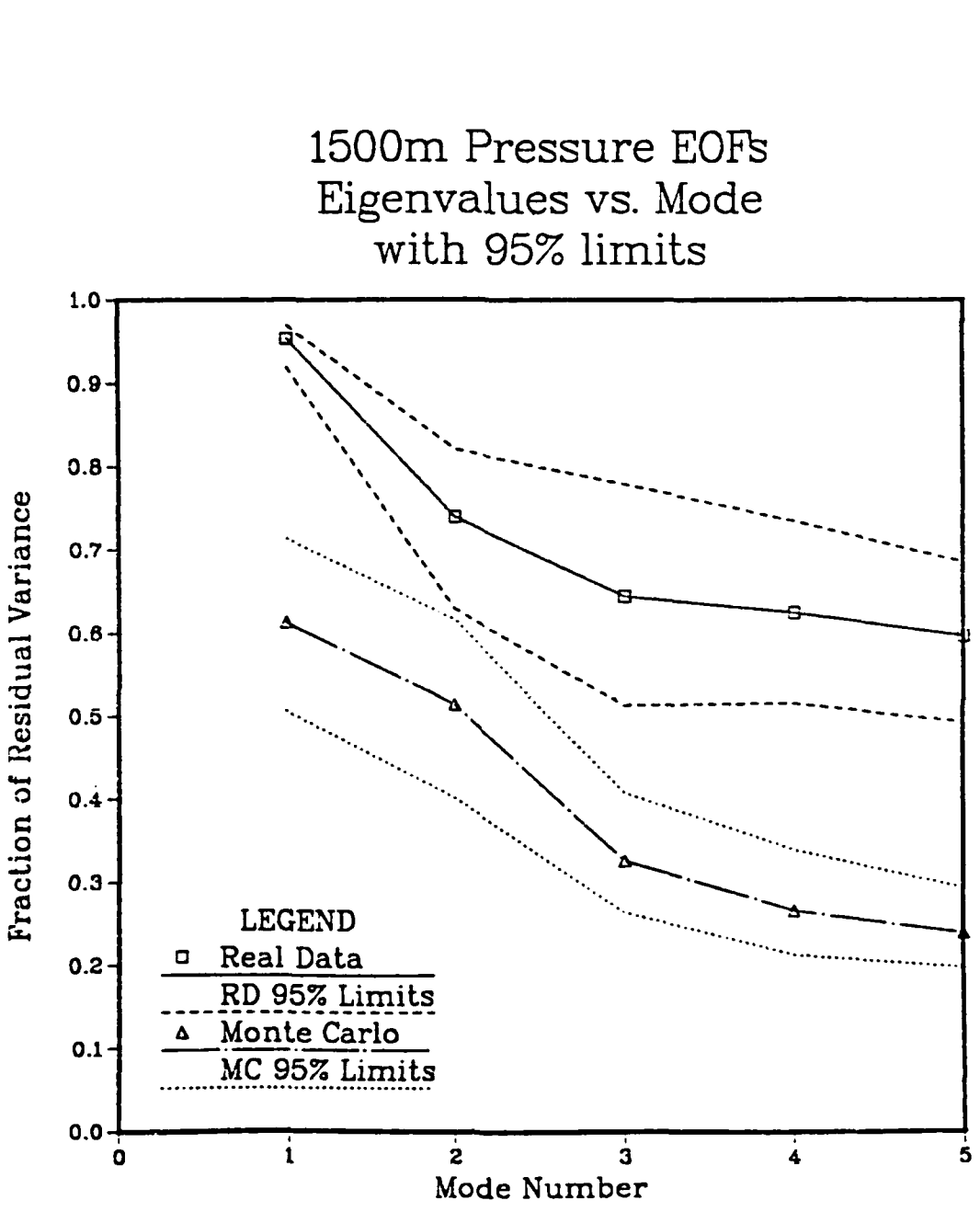

Comparison of the fraction of residual pressure variance accounted for by each mode compared to the fractions accounted for in the case of pure noise in the density measurements. Note how much variance the pure noise analysis puts into the first pressure mode; yet not even the 95% confidence limits overlap with the real data.

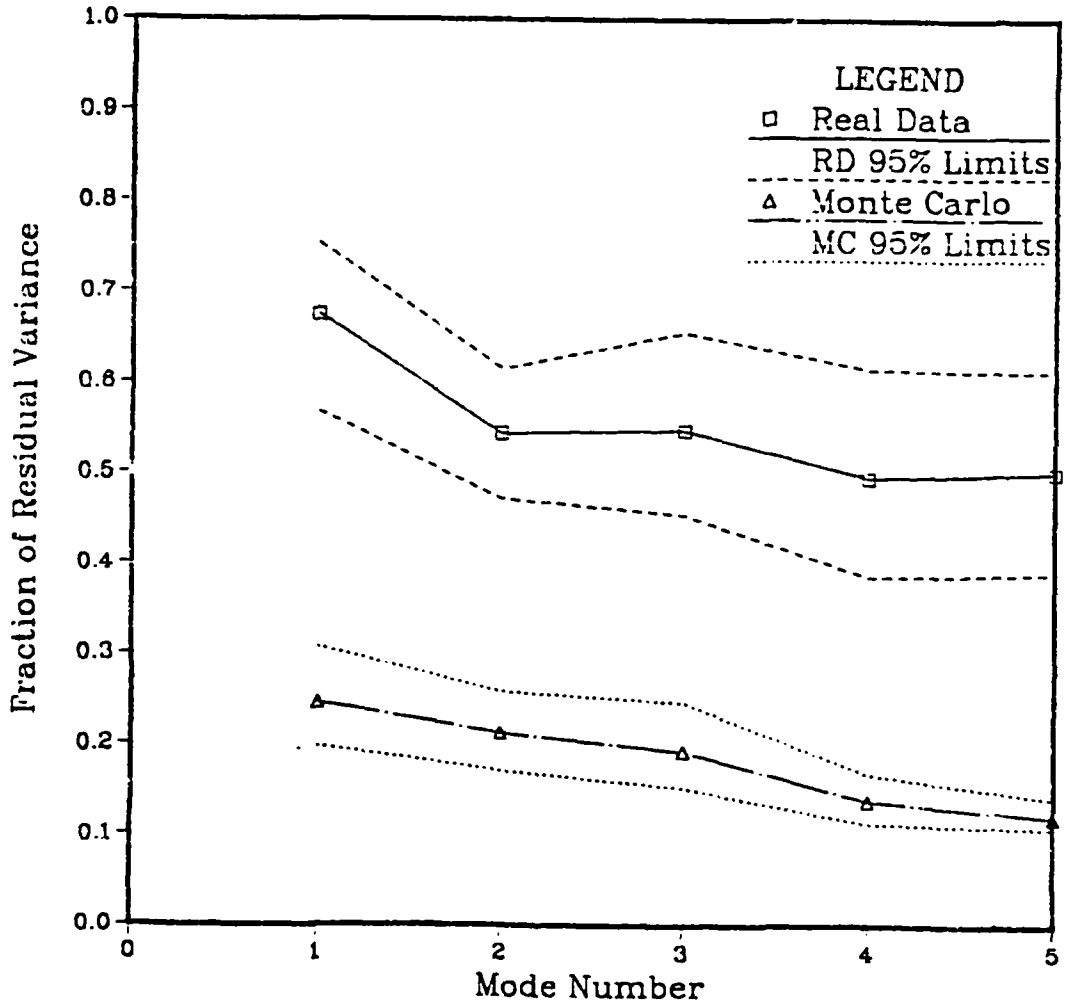

10 As in 9, but for the density modes. Again, note that the real data is so 'noise-free' that even the 95% confidence limits don't overlap.

Each survey had enough casts to 500m or more to form independent estimates of the EOFs to that depth (see Table 1). The first pressure EOF accounts for 90 to 99.4% of the pressure variance in the top 500m, while the first density EOF accounts for 59% to 95% of the density variance to that depth (see Table 3 and Figures 11 and 12). The surveys with a more clearly defined near-surface mixed layer (e.g., OPTOMA4-1) are also less well described by a single EOF. The mixed-layer structure, when present, is clearly seen in the EOFs of density variance, as well as in the mean profiles and density QGMs (see Figures

Table 3.

Variance captured in first EOF, by survey.

survey:	opt2	opt4-1	opt4-2	opt5-a1	opt5-a3	opt5-d
%var. in 500m EOF(1):						
pressure	98.10	88.65	97.36	99.45	91.01	96.09
density	87.38	75.83	74.61	90.84	75.17	72.29
#profiles	66	25	26	6	18	28
%var. in 1500m EOF(1):						
pressure	96.14	79.48	97.18	-	-	96.44
density	80.34	84.09	73.85	-	-	77.23
#profiles	9	8	8	-	-	8

2,5,12). The EOFs appear to be fairly robust below 150 meters or so.

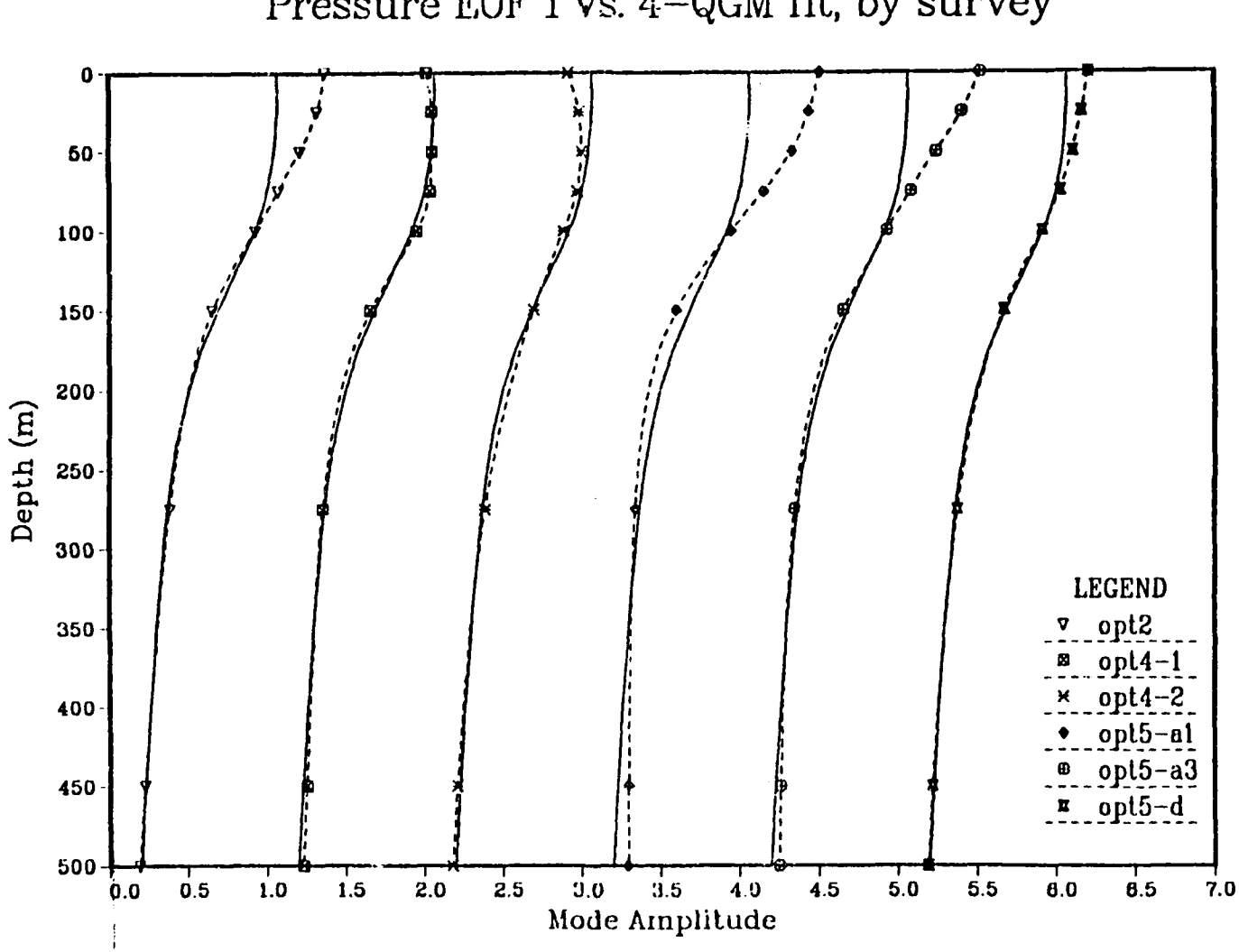

11 The first pressure EOF from each survey (dotted lines), from all casts to 500m or greater. The solid lines represent the least-square-fits by the first four QGMs of OPTOMA5-D.

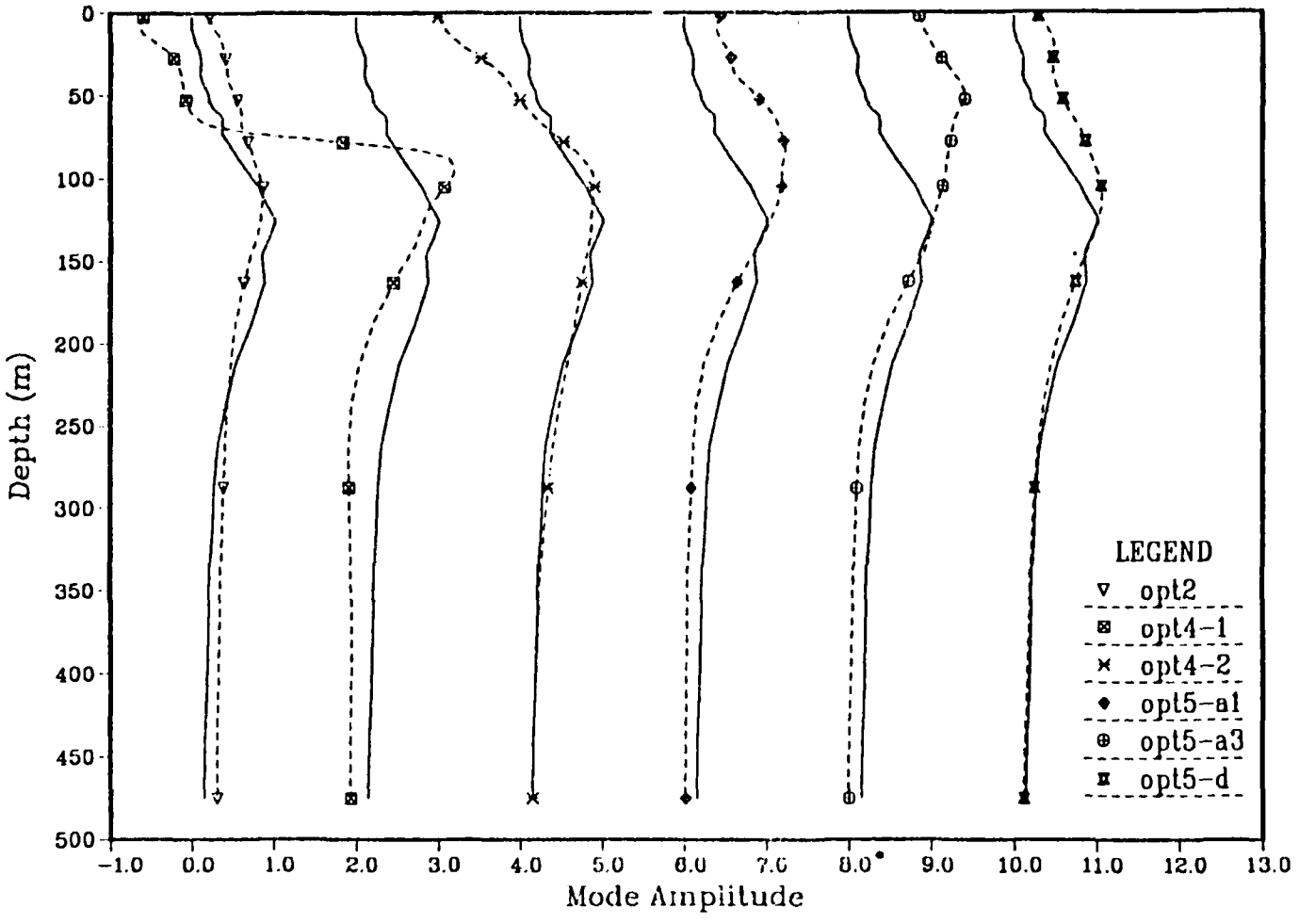

12 The first density EOF from each survey, from all casts to 500m. The solid line profiles represent the fits by four QGMs from OPTOMA5-D.

The EOFs are only defined where there are data; i.e., over the subranges 0 to 500m, 0 to 1500m, or 0 to 3000m; and they are orthogonal over that interval. The QGMs are orthogonal over the total depth, but not over lesser intervals. To compare the EOFs with the QGMs, therefore, least squares fits were performed. Both the EOFs and QGMs are normalized so that the squared integral equals the appropriate depth; this allows depth-by-depth comparison of the values of EOFs formed to different depths, without requiring conversion factors. Since the effects of surface mixing may "contaminate" the results in the top few tens of meters, the least-squares fits were repeated, excluding data above a "mixed layer depth" (varying between 0 and 150m).

The resulting coefficients are robust (within 2%) for fits applied over intervals from (0,3000) to (150,3000) and also for fits performed over the ranges (0,1500) to (150,1500). However, the coefficients are not quite the same for the 1500m fit vs. the 3000m fit. The first 3000m EOF, when fit over just the upper 1500m, yields roughly the same coefficients as for the actual 1500m EOF 1; hence, this difference is probably due to the definition of structure to a greater depth rather than to anomalous behavior in the eight deep casts. The coefficients are not robust for fits performed to only 500m (the depth of most casts to date). This is probably due to the significant crosstalk between the QGMs in this depth subrange (see Table 1 again). In view of this, it will probably be necessary to restrict the interpretation of 500m (or less) data to just the

lowest modes; e.g., QGM 1 and (maybe) 2. The coefficients from the 1500m and 3000m fits of the pressure EOFs 1 to 4 by QGMs 1 to 5 are

Table 4.

(A) Least squares fits of pressure EOFs by QGMs, 100 to 3000m:

QGM:		1	2	3	4	5
EOF	% goodness					
1	99.97	0.927	0.101	0.084	-.011	-.020
2	99.72	-.144	0.837	0.359	0.020	0.077
3	97.37	-.120	-.296	0.250	0.659	0.120
4	86.35	0.160	0.100	-.173	0.007	0.835

(B) Least squares fits of pressure EOF by QGMs, 100 to 1500m:

QGM:		1	2	3	4	5
EOF	% goodness					
1	99.99	1.025	-.032	0.112	-.032	-.001
2	99.96	-1.322	1.248	-.206	0.166	-.012
3	99.72	1.222	-1.256	0.850	-.076	0.276
4	99.57	-2.774	1.363	-1.894	0.287	-.194

given in Table 4. Note that the fourth and fifth baroclinic QGMs do not contribute much to the fit of EOF 1.

For comparison, a 4-mode fit, using the 100 to 3000m fitting data (from OPTOMA5-D), is shown with the 500m pressure EOFs from each

survey in Figure 11. The 500m density EOFs are shown in Figure 12, again with the 150-3000m density QGM fit from the eight deep casts. Although the EOFs display considerable variability near the surface, the fit of EOFs below 100 meters or so is fairly good, even using 'standard' QGMs (defined, in this case, by the eight casts to 3000m). The variations shown in Figure 12 appear comparable with those of the QGMs themselves, shown in Figure 5. This is quite encouraging; especially with respect to the (dynamically significant) pressure variations.

V. Mode Independence and QG Dispersion.

There is no constraint on the QGM amplitudes $A_n(x,y,t)$; yet, as mentioned above, the amplitudes of the EOFs are constrained to be uncorrelated. To evaluate whether it is reasonable to expect the QGMs to be uncorrelated over the study region, it is useful to examine the linear dispersion relation.

In the absence of other currents, the dispersion relation for a single planetary (Rossby) wave of (intrinsic) frequency ω, wavenumber $\underset{\sim}{k}=(k_m\cos\alpha, k_m\sin\alpha)$, and mode m is:

$$\omega = \frac{\beta k_m \cos\alpha}{\lambda_m^2 + k_m^2}$$

where $\beta = \partial f/\partial y$ is the variation of the coriolis parameter with latitude, λ_m^2 is inverse of the m-th internal Rossby radius, and α is the angle between $\underset{\sim}{k}$ and due west.

Rearranging for k_m in terms of ω yields:

$$k_m = R^{-1}\{1 \pm \sqrt{1 - R^2\lambda_m^2}\}$$

where

$$R(\omega,\alpha) = \frac{2\omega}{\beta \cos\alpha}$$

is a characteristic length for the frequency ω and northward deflection α.

For k_m to be entirely real, ω must be less than the maximum frequency $\omega_m = (\beta \cos\alpha)/(2\lambda_m)$. At this maximum frequency, $k_m = 1/(R(\omega_m,\alpha)) = \lambda_m$. Table 5 shows, for modes 0 to 4 and for $\alpha = 0°$, the minimum periods $T_m = 2\pi/\omega_m$, the internal Rossby radii λ_m^{-1}, the wavelength $2\pi\lambda_m^{-1}$ associated with T_m, and the corresponding phase speed

Table 5.

(linear QG modal wave parameters)

mode:	0	1	2	3	4
T_m (days)	3.8	340	626	916	1,251
λ_m^{-1} (km)	2,160	24	13	8.9	6.5
$2\pi\lambda_m^{-1}$ (km)	13,500	150	82	56	41
c_m (cm/sec)	4,140	0.51	0.15	0.07	0.04

c_m. (The value of β used is appropriate to 38N).

A striking feature is the long time scales associated with the baroclinic modes. Even the first baroclinic mode has a minimum period of

almost a year, corresponding to a phase speed of .51 cm/sec. Apparently, even a relatively weak current would overwhelm phase propogation, and hence advection must be important.

In the study region, there is a climatological mean southerly flow of several cm/sec roughly parallel to the coast (Chelton, 1984). Although this is "weak" in comparison to, say, a western boundary current, it is certainly "strong" in comparison to the above phase speeds of less than 0.5 cm/sec. Further, the observed currents including mesoscale features resolved in the listed surveys can exceed 50 cm/sec (Mooers and Robinson, 1984). In view of this, the validity of using linear phase speeds is cast into doubt (since two or more Rossby waves are not an exact solution of the QG equations). Nevertheless, we shall make use of the linear dispersion relation in the third and fourth scenario considered below: (iii) the wake of a feature embedded in a large-scale mean flow (e.g., southerly flow over the east-west oriented Mendocino escarpment), and (iv) forcing at fixed frequencies.

(i)

As a first scenario, suppose the significant activity present in each mode is near the internal Rossby radius of deformation, $k_m = \lambda_m$ (e.g., due to baroclinic instability). Then, since the adjacent modes have Rossby radii differing by nearly a factor of 2 (see Table 5), the modes should separate in about one mode-1 wavelength, no matter what the orientation or the degree of nonlinearity (i.e. about 150 km).

(ii)

Next, consider a field of "eddies"; i.e. where non-linear effects totally dominate the dispersion. It is plausible that the eddies (and meanders) can have axes tilted from the vertical (e.g. due to a shearing mean flow, or to interactions with the bottom or with each other). In a modal representation, this tilting would translate into a spatial displacement of the modal coefficients. For example, an eddy of uniform strength in depth but with an axis tilted from the vertical would yield two equal but opposite baroclinic 'eddies' situated symmetrically about a single central barotropic 'eddy'. (The centers of the baroclinic 'eddies' would be located roughly at the edge of the region of nearly solid-body rotation; the relative strength of the baroclinic portion depends on the degree of tilt of the axis.) This would tend to induce spatial quadrature between the modes, and hence low correlation at zero spatial lag. Since the "statistical independence" imposed on the EOFs means only no zero-lag (in space and time) correlation, the envisioned field of eddies with tilted axes would then roughly satisfy the constraint. (It is noteworthy that McWilliams and Shen (1980) observed near quadrature between the barotropic and first baroclinic modes in the MODE-1 data set).

(iii)

Now consider a mean current from an angle "γ" north of west, flowing with strength "V" over a topographic feature such that there is

a Rossby-wave wake with a fixed wavenumber $k=\ell$, and with phase lines held stationary by the current. Substituting this value of k into the equation for phase speed, and solving for α, the northward deflection angle of the Rossby wave such that the phase lines are held stationary by V, we obtain:

$$\tan\alpha = (c_m/V - \cos\gamma)/\sin\gamma ,$$

where $c_m = \beta/(\lambda_m^2+\ell^2)$ is the westward speed at which the intersection of a phase line of the wave and an E-W oriented line propagates (no matter what the value of 'α'). For roughly southerly flow, $\sin\gamma$ is near one and $\cos\gamma$ is near zero; for $V>>c_m$, the angle between the phase lines of (say) the mode 1 and mode 2 solution is then roughly $V/(c_1-c_2)$. The downstream distance "D" required to observe a full cycle phase shift between modes 1 and 2 would be

$$D = 2\pi\lambda_1^{-1}(V/(c_1-c_2)).$$

Physically, after the mean flow has advected the waves southward some distance D the westward propagation speeds c_1 and c_2 have separated the two modes in an E-W direction by some distance (c_1-c_2) times the elapsed time, T=D/V. A full cycle difference is achieved when the phase-line separation in the E-W direction equals the distance between the crests of the waves. For a mean southerly flow of around 5 cm/sec, for example, D becomes about ten times the (observed) wavelength (which, in the study region, would be about 1500 km). This is roughly three times the extent of the study region; hence, if this scenario were valid, we would expect to see fairly strong coherence between the modes.

(iv)

Finally, consider forcing at fixed frequencies. The long times associated with the intrinsic periods (a year or more) imply that Doppler shifting by large scale mean advection is likely to be important. This view is supported by the variations between surveys, which indicate significant qualitative changes in both strength and scale of the motion on a seasonal basis (see also Chelton 1980). Although annual-period Rossby waves are almost certainly present near the study region (Kang and Magaard 1980, White and Saur 1981, Mysak 1983), such motions would appear, in the present set of surveys, as large-scale, time-mean flows, and hence are not directly of interest. For simplicity, consider a mean flow exactly from north to south, with strength "V"; then add periodic forcing at some point (e.g., at the corner where the Mendocino escarpment meets the shelf) with some frequency "σ". For a given northward deflection "α", the equation describing the Doppler shift is

$$\sigma = \frac{\beta k_m \cos\alpha}{\lambda_m^2 + k_m^2} + V k_m \sin\alpha .$$

To accommodate frequencies much larger than the maximum intrinsic frequency allowed, the second (Doppler shift) term on the right must dominate over the first. The resulting wavenumber, $k = \sigma/V \sin\alpha$, is then approximately independent of the mode. Physically, the downstream distance from crest to crest is simply set by the distance the current flows in one forcing period. For forcing with periods much less than a year (e.g., for observed periods of the order of weeks), this mechanism would thus also produce strong coherence between the various modes.

The tentative conclusion is that, of the mechanisms reviewed here, only the first two produce motions where the amplitudes of the different modes appear uncorrelated: (i) generation at the scale of the Rossby radii, or (ii) non-linear dynamics involving "tilted axes". Some fraction of the variance found in each mode may be due to internal wave action (e.g., internal tides). The differences in the phase speeds of the different internal wave modes at tidal frequencies is sufficient that these too might be expected to produce uncorrelated modal coefficients over the survey domains. If all of the above mechanisms are active to some degree, then the actual correlation between modes could have almost any value.

VI. Discussion.

(A) Modal Structure.

The first four pressure EOFs to 3000m, based on only eight casts to that depth, look quite similar to the dynamic modes. 3000m is close enough to the total water depth that it is, perhaps, acceptable that the orthonormality condition in depth doesn't interfere with this correspondence. In addition, however, the required independence of the EOF amplitudes could interfere. If all of the mechanisms for generation reviewed in the last section were active, we might expect to see some correlated and some uncorrelated activity among the various dynamic modes. Even for two unrelated stochastic processes, sampling error

would be expected to introduce an artificial correlation. For example, an estimate based on 8 samples with the mean removed would give an expected value of 1/7 for C^2, where $C=\langle xy\rangle/(\langle x^2\rangle\langle y^2\rangle)^{1/2}$ is the measured correlation; i.e. the expected magnitude of C (of either sign) is around 0.4. It therefore seems sensible to ask how much correlation between modes can be tolerated, and yet still produce EOFs which appear similar to the QGMs.

As noted previously, the rapid dropoff of variance with mode number can account for the correspondence between the EOFs and QGMs, in spite of some amount of real or artificial correlation. Consider (for example) a 2-dimensional case, where the two basis vectors are taken as Φ_1 and Φ_2. Then imagine a cloud of points, each representing the $(A_1, A_2)=(x,y)$ amplitude pair for a 'station'; this cloud could be described, for example, by an ellipse defining the root mean square (rms) distance from the centroid (at the origin for demeaned data). The EOFs represent axes rotated so that the x' axis (say) is aligned with the major axis of this ellipse, and the y' axis perpendicular; i.e. so that $\langle x'y'\rangle=0$. The counter-clockwise angle of rotation 'θ' which yields $\langle x'y'\rangle=0$ is given by

$$\tan 2\theta = 2\langle xy\rangle/(\langle x^2\rangle-\langle y^2\rangle).$$

Now suppose that the variance in (say) the x-direction is about 4 times that in the y-direction, and that the x-y correlation C (as defined above) is 0.5. The major axis of the "rms ellipse" would then be tilted

about 9.2 degrees from the x-axis; the x',y' axes (or EOFs) would thus be only slightly different from the original x,y axes. In the case described (not too different from the actual pressure mode case), the first EOF would be comprised of about 97.4% QGM 1 and 2.6% QGM 2 (using 'percent goodness of fit', as defined above); it would 'explain' 91.1% of the total variance (compared to 80% in QGM 1 alone). The second EOF, conversely, would be 97.4% QGM 2 and 2.6% QGM 1, and would capture the remaining 8.9% of the variance.

The comparison with shallower EOFs can also be examined in this simplified example. The truncation of the QGMs to shallower depths corresponds to taking a projection of higher-dimensional vectors onto a lower-dimensional space. For example, sampling the first two QGMs at just two depths will allow any two-point profile to be described, but (i) all the activity in higher modes is aliased in, and (ii) the two QGMs may not be orthogonal (with respect to a two-layer "integration"). If the drop in variance with mode is sufficiently drastic, the first effect might not be a problem; in this case, the first QGM and EOF would still appear quite similar. However, the second QGM and EOF could be forced by the orthogonality constraints to be quite different.

(B) Surface mixing.

As mentioned previously, the top 100m or so of both the QGMs and EOFs display much variability from survey-to-survey (see Figures 5,

12). Although the deeper part (below 150 meters) is suitably robust, this variability near the surface will contribute to the unpredictability of the actual surface flow. In the two extreme examples in Figure 11, for instance, the mode 1 value for the pressure anomaly at the surface differs by a factor of about two. This translates directly to a factor of two uncertainty in the magnitude of the geostrophic current to be found there. Near the surface, the currents are also strongly affected by the wind (e.g., Ekman drift, inertial currents). The response to the wind is also sensitive to the near-surface density profile (i.e., the depth of the 'mixed layer'). These two effects may reinforce each other to degrade our ability to describe and predict currents at the ocean surface. This near-surface variability may also play a significant part in the energy budget for the baroclinic QG activity, since QGMs 2 and higher have zero-crossings in the upper 250m of the water column.

The near-surface features are suggestive of mixing effects. For example, the well-defined mixed layer in OPTOMA4-1 is visible in the EOF of density variability; i.e., the density of the homogeneous layer varies, and the density fluctuations are somewhat correlated with the deeper variations. Surprisingly, this correlation, in the case of OPTOMA4-1, seems to be negative (see Figure 12). A possible explanation is that when the denser water below is brought nearer to the surface by the quasi-geostrophic flow, the same amount of mixing induces greater density at the surface than under average conditions;

likewise, when the near-surface density profile is stretched by the quasi-geostrophic motions, the same amount of mixing induces less of an increase in surface density than on the average. In an area containing several mesoscale features, this would result in an initially positive correlation between the underlying QG density field and the density of the mixed layer. Subsequent quasi-geostrophic evolution could then reverse the phase of the underlying density variations, while the mixed layer variations remain frozen or change little (as, perhaps, in survey opt4-1, Figure 12).

Alternatively, the advection of surface water from the coastal region or from offshore should be considered. In particular, satellite IR images sometimes show well defined cold surface features extending offshore and apparently wrapping around mesoscale features in the area (e.g., Mooers and Robinson 1984). In such cases, the correlation most clearly visible associates the cold surface water with currents; i.e., with the horizontal *gradient* of the QG density field, rather than with the subsurface density variations themselves. This would tend to impose quadrature upon the surface to depth correlations. Subsequent horizontal advection of the mixed layer (for example, by Ekman drift) could then induce a non-zero correlation with the underlying field, of either sign.

(C) Topographic Rossby waves.

The ocean bottom in the survey area may be more accurately modelled as a gently sloping plane (the typical slope is about 400m in 100 Km, out of a total depth of 4000m); hence there may be topographic Rossby waves. The signature of baroclinic topographic waves is bottom trapping. Although there is some suggestion of increased activity at the deep ends of the third and fourth EOFs to 3000m, the activity indicated is very small (and within the 95% limits of zero). In view of this, it would seem extravagant to calculate the topographic modes. If we had more data nearer the bottom, it might then become worthwhile to examine topographic effects in more detail.

VII. Summary.

The main conclusions of this work are as follows:

(1) The first four empirical modes (EOFs) of pressure perturbations appear quite similar to the first four quasi-geostrophic modes (QGMs). This correspondence becomes tighter as the depth to which the data (and hence EOFs) approaches the total water depth. The differences are most likely attributable to the different depths over which the orthogonality constraint is imposed.

(2) The perturbation variance contained in each dynamic mode decreases sharply with mode number. Because of this, the statistical

independence imposed on the EOF modal amplitudes does not interfere with the above correspondence to the QGMs.

(3) The first few QG modes can be separated effectively in 3000m CTD data, and fairly effectively in 1500m CTD data. The interpretation of shallower cast data, however, should either be limited to the first baroclinic mode, or an alternate method (rather than direct least-squares fitting) should be applied.

ACKNOWLEDGEMENTS

The author would like to thank the many people without whose work this would not have been possible; however, a limited sample will have to suffice. A special thanks to C.N.K Mooers and A.R. Robinson, who were chief scientists on some of the surveys mentioned, and whose criticisms and comments were invaluable. I also thank Dr. M.M. Rienecker and Ms. M.C. Colton, for performing some quality control and editing of the data, and for the many discussions concerning the quality and meaning of the same. This work was supported by the Physical Oceanography Program of the Office of Naval Research.

REFERENCES

Chelton, D.B., 1984: Seasonal variability of alongshore geostrophic velocity off central California. (to appear in *J. Geophys. Res.*)

Davis, R.E., 1977: Techniques for statistical analysis and prediction of geophysical fluid systems, *Geophys. Astrophys. Fluid Dyn.*, *8*:245-277.

Diaconis, and B. Efron, 1983: Computer-intensive methods in statistics. *Scientific American*, *248*(*5*): , (May 1983).

Efron, B., 1979: Computers and the theory of statistics: thinking the unthinkable. *SIAM Review*, *21*(*4*):460-480.

Emery, W.J., 1975: Dynamic height from temperature profiles. *J. Phys. Oceanogr.*, *5*:369-375.

Emery, W.J., and R.T. Wert, 1976: T-S curves in the Pacific and thier application to dynamic height computation. *J. Phys. Oceanogr.*, *6*:613-617.

Flierl, G.R., 1978a: Correcting expendable bathythermograph (XBT) data for salinity effects to compute dynamic heights in Gulf Stream rings. *Deep Sea Res.*, *25*:129-134.

Flierl, G.R., 1978b: Models of vertical structure and calibration of two-layer Models. *Dyn. Atmos. Ocean*, *2*:341-381.

Kang, Y.Q., and L. Magaard 1980: Annual baroclinic Rossby waves in the central North Pacific. *J. Phys. Oceanogr.*, *10*:1159-1167.

Lewis, E.L., and R.G. Perkin, 1978: Salinity, its definition and calculation. *J. Geophys. Res.*, *83*:466-478.

Lorentz, E.N., 1956: Empirical Orthogonal Functions and Statistical Weather Prediction. Scientific Report no. 1, Statistical Forecasting Project, M.I.T.

Mardia, K.B., J.T. Kent, and J.M. Bibby, *Multivariate Analysis*. Academic Press, 1979.

McWilliams, J.C., 1976: Maps from the Mid-Ocean Dynamic Experiment: Part I. Geostrophic Streamfunction. *J. Phys. Oceanogr.*, *6*:810-827.

McWilliams, J.C., and G.R. Flierl, 1975: Quasi-geostrophic wave analysis of MODE array data. In *Dynamics and the analysis of MODE-I*, A.R. Robinson, editor. Mass. Inst. Tech., 54-1417, Cambridge, 250 pp.

McWilliams, J.C., and G.R. Flierl, 1976: Optimal, quasi-geostrophic wave analysis of MODE array data. *Deep-Sea Res.*, *23*:285-300.

McWilliams, J.C., and C.Y. Shen, 1980: Mesoscale Modal Coupling. *J. Phys. Oceanogr.*, *10*:741-752.

Miller, R.N., A.R. Robinson, and D.B. Haidvogel, 1983: A baroclinic quasigeostrophic open ocean model. *J. Comp. Phys.*, *50*:38-70.

Millero, F.J., C.T. Chen, A. Bradshaw, and K. Schleicher, 1980: A new high pressure equation of state for seawater. *Deep Sea Res.*, *27*A:255-264.

Mooers, C.N.K., and A.R. Robinson, 1984: Turbulent Jets and Eddies in the California Current and Inferred Cross-Shore Transports. *Science*, *223*:51-53.

Mysak, L.A., 1983: Generation of annual Rossby waves in the North Pacific. *J. Phys. Oceanogr.*, *13*:1908-1923.

Preisendorfer, R.W., 1980: Principal Components and the Motions of Simple Dynamic Systems. SIO Reference series 81-4, Scripps Inst. of Oceanography.

Preisendorfer, R.W., F.W. Zwiers, and T.P. Barnett, 1981: Foundations of Principal Component Selection Rules. SIO Reference series 81-4, Scripps Inst. of Oceanography.

Rienecker, M. M., C.N.K. Mooers, M.C. Colton, and P.A. Wittmann, 1984: Hydrographic data from the OPTOMA program: OPTOMA2, Legs I and II. NPS technical report NPS68-84-002, Naval Postgraduate School.

Robinson, A.R., L.J. Walstad, E.F. Carter, M.M. Rienecker, J.A. Smith, and W.G. Leslie, 1984: A Real Time Dynamical Forecast of Ocean Synoptic/Mesoscale Eddies. *Nature* (*in press*).

Smith, B.T., *et al.*, 1976: Lecture notes in Computer Science *6*: Matrix Eigensystem Routines- Eispack Guide. Springer-Verlag, New York. (Programs are available from the National Energy Software Center, Argonne National Laboratories, or through International Mathematical and Statistical Libraries (IMSL), inc.).

White, W.B., and J.F.T. Saur 1981: A source of annual baroclinic waves in the eastern subtropical North Pacific. *J. Phys Oceanogr.*, *11*:1452-1462.

INITIAL DISTRIBUTION LIST

Defense Technical Information Center Cameron Station Alexandria, VA 22314	2
Dudley Knox Library Code 0142 Naval Postgraduate School Monterey, CA 93943	2
Office of Research Administration Code 012 Naval Postgraduate School Monterey, CA 93943	1
Prof. C.N.K. Mooers Chairman, code 0068 Department of Oceanography Naval Postgraduate School Monterey, CA 93943	15
Dr. J.A. Smith Department of Oceanography Naval Postgraduate School Monterey, CA 93943	50
Dr. M.M. Rienecker Department of Oceanography Naval Postgraduate School Monterey, CA 93943	1
Ms. M.C. Colton Department of Oceanography Naval Postgraduate School Monterey, CA 93943	1
Mr. P.A. Wittmann Department of Oceanography Naval Postgraduate School Monterey, CA 93943	1
Prof. A.R. Robinson Center for Earth and Planetary Physics Pierce Hall, Harvard University Cambridge, MA 02138	5

Dr. E.V. Carter 1
Center for Earth and Planetary Physics
Pierce Hall, Harvard University
Cambridge, MA 02138

Dr. J. Carton 1
Center for Earth and Planetary Physics
Pierce Hall, Harvard University
Cambridge, MA 02138

Mr. L. Walstad 1
Center for Earth and Planetary Physics
Pierce Hall, Harvard University
Cambridge, MA 02138

Ms. N. Pinardi 1
Center for Earth and Planetary Physics
Pierce Hall, Harvard University
Cambridge, MA 02138